Perrhenate Incorporation into Binary Mixed Sodalites: The Role of Anion Size and Implications for Technetium-99 Sequestration

Johnbull O. Dickson[*1], James B. Harsh[1], Wayne W. Lukens[2], and Eric M. Pierce[3],

[1]Department of Crops and Soil Sciences, Washington State University, P. O. Box 646420, Pullman, WA 99164, USA

[2]Chemical Sciences Division, Lawrence Berkeley National Laboratory, Berkeley, CA 94720

[3]Environmental Sciences Division, Oak Ridge National Laboratory, P. O. Box 2008, Oak Ridge, TN 37831.

*Corresponding Author: J.dickson@wsu.edu

Abstract

Perrhenate (ReO_4^-), as a TcO_4^- analogue, was incorporated into mixed-anion sodalites from binary solutions containing ReO_4^- and a competing anion X^{n-} (Cl^-, CO_3^{2-}, SO_4^{2-}, MnO_4^-, or WO_4^{2-}). Our objective was to determine the extent of solid solution formation and the dependence of competing ion selectivity on ion size. Using equivalent aqueous concentrations of the anions (ReO_4^-/ X^{n-} molar ratio = 1:1), we synthesized mixed-anion sodalites from zeolite and NaOH at 90°C for 96 h. The resulting solids were characterized by bulk chemical analysis, powder X-ray diffraction, scanning electron microscopy, and X-ray absorption near edge structure (XANES) spectroscopy to determine crystal structure, chemical composition, morphology, and rhenium (Re) oxidation state. Rhenium in the solid phase occurred predominately as $Re(VII)O_4^-$ in the

sodalites, which have a primitive cubic pattern in the space group $P\bar{4}3n$. The refined unit-cell parameters of the mixed sodalites ranged from 8.88 to 9.15 Å and showed a linear dependence on the size and mole fraction of the incorporated anion(s). The ReO_4^- selectivity, represented by its distribution coefficient (K_d), increased in the following order: $Cl^-<NO_3^-<MnO_4^-$ and $CO_3^{2-}<SO_4^{2-}<WO_4^{2-}$ for the monovalent and divalent anions, respectively. The relationship between the ReO_4^- distribution coefficient and competing anion size was nonlinear. When the difference in ionic radius (DIR) between ReO_4^- and X^{n-} (*n = 1 or* 2) was greater than ~12%, then ReO_4^- incorporation into sodalite was insignificant. The results imply that anion size is the major factor that determines sodalite anion compositions. Given the similarity in chemical behavior or anion size when redox is not concerned ReO_4^- is likely to serve as a suitable analogue for TcO_4^- where Tc(VII) is the stable oxidation state.

Highlights

- Mixed-anion sodalites were synthesized from zeolite and NaOH at 90°C
- Solid solution formation and ion selectivity were studied
- Solid phases were characterized by chemical analysis, XRD, SEM, and XANES
- Perrhenate selectivity for the mixed-anion sodalite cages increased in the following order: $Cl^-<NO_3^-<MnO_4^-$ and $CO_3^{2-}<SO_4^{2-}<WO_4^{2-}$
- The influence of anion size on mixed-anion sodalite compositions was documented

Keywords

Mixed-anion sodalites; Anion selectivity; Distribution coefficient; Perrhenate; Pertechnetate, Technetium-99; Nuclear waste

1. Introduction

The safe disposal of nuclear waste generated by the nuclear fuel cycle remains one of the most challenging and potentially costly environmental endeavours facing the nuclear energy industry (Ewing, 2006). Additionally, disposal of reprocessed waste generated as a result of the Cold War legacy remains a challenge for numerous industrialized nations (Ewing, 1999). The application of versatile porous framework materials (feldspathoids) as a selective medium for sequestration of long-lived anionic radionuclides (e.g., $^{99}TcO_4^-$, $^{129}I^-$, $^{75}SeO_4^{2-}$) represents a key component of a closed nuclear fuel cycle. Furthermore, advanced knowledge of factors governing anion selectivity in feldspathoids is critical for their potential application in anion-sequestration processes (Custelcean and Moyer, 2007).

Feldspathoids such as cancrinite and sodalite (Fig. 1) have crystalline microporous framework structures. They can be represented by the general formula: $A_8[TO_4]_6X_2$ where T is Al and/or Si, and A and X are monovalent or divalent cations and anions, respectively (Taylor and Henderson, 1978). Sodalite, a high-temperature, low pressure phase, consists of corner sharing SiO_4 and AlO_4 tetrahedra constructed into four and six-membered rings that form the cuboctahedral cages referred to as sodalite β-cages. The sodalite framework can be considered as a space-filling arrangement of the sodalite β-cages directly linked via the six-membered rings to form the semi-condensed sodalite structure. In the center of the cage is an anion that is tetrahedrally coordinated to four cations, forming A_4X clusters (Trill, 2002). Because anions are strongly trapped within the cages natural or synthetic sodalite phases constitute highly durable waste forms for immobilization of key anionic radionuclides (Maddrell et al., 2014).

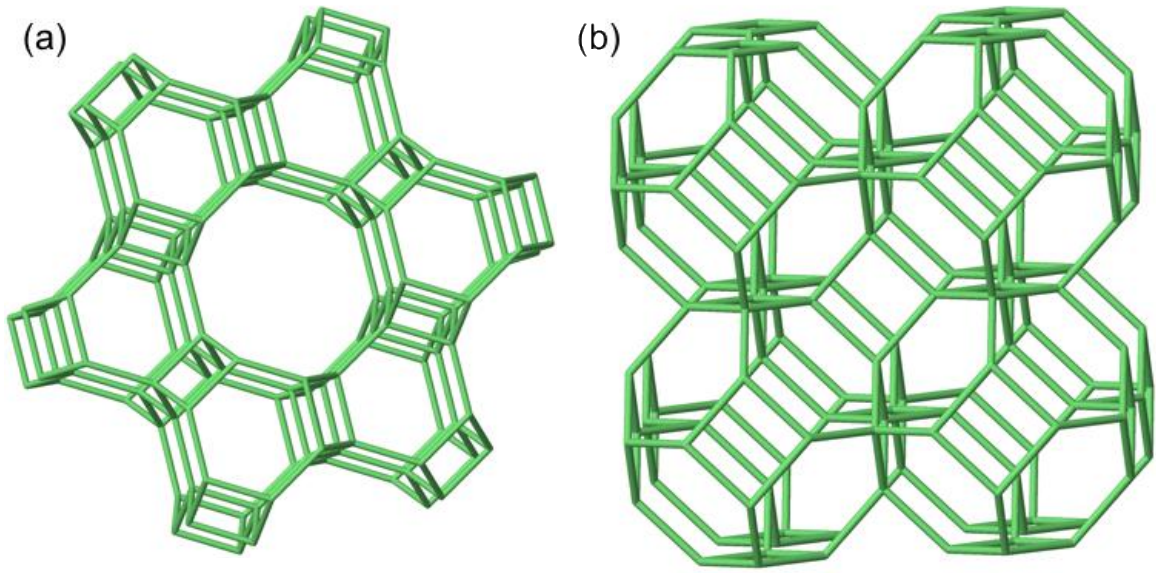

Fig. 1. (a) Cancrinite structure (ABABAB…. stacking sequence). (b) Sodalite structure (ABCABC… stacking sequence of the six-rings)(Baerlocher and McCusker, 2014). For clarity cage oxygen, anions and cations were omitted.

Feldspathoids with guest ions in their structure have been widely studied (Johnson et al., 1999). Most studies have been devoted to mixed cation substitutions in sodalite frameworks (Brenchley and Weller, 1994; Stein et al., 1992) and to single anion sodalites (Weller and Wong, 1989; Weller et al., 1990), but the substitution of multiple guest anions in mixed sodalite phases is not well understood. Research into sodalite selectivity for anionic species of varying sizes is important for elucidating anion substitution into mixed sodalites with more complex structures, especially those sodalites containing key anionic radionuclides ($^{99}TcO_4^-$, $^{129}I^-$, $^{75}SeO_4^{2-}$). Significant gaps exist in our current understanding of the role of sodalite selectivity as a driving force for controlling anion incorporation into the structure.

Previous work with NO_3/ReO_4-sodalites suggests that selectivity might be anion size-dependent (Dickson et al., 2014), but there is lack of experimental evidence

demonstrating the selectivity of different ions for incorporation into sodalites. Therefore, we investigated under oxidizing conditions the competitive incorporation of ReO_4^- into mixed anion-bearing sodalites in the presence of these competing anions (X^{n-}) ranging in size and charge: Cl^-, CO_3^{2-}, SO_4^{2-}, MnO_4^-, and WO_4^{2-}.

We used Re as a nonradioactive analogue for Tc because both elements occur primarily under oxidizing conditions as oxyanions (ReO_4^- and TcO_4^-), which have similar metal oxygen bond lengths (Tc–O = 1.702 Å; Re–O = 1.719 Å) and ionic radii (TcO_4^- = 2.52 Å; ReO_4^- = 2.60 Å)(Icenhower et al., 2010; Marcus, 1991; Moyer and Bonnesen, 1979). However, in reducing environments, the redox chemistry of Re and Tc significantly differs due to the difference in standard electrode potentials (E_h) of the two species (ReO_4^-/ReO_2 = 0.510 V and TcO_4^-/TcO_2 = 0.738 V), and ReO_4^- being more difficult to reduce than TcO_4^- (Darab and Smith, 1996; Lukens et al., 2007; Wakoff and Nagy, 2004). For example, at pH 8, the E_h would have to drop below 0.25 V before $TcO_2 \cdot 2H_2O(s)$ would form in the presence of 10^{-8} *M* TcO_4^- (Icenhower et al., 2010) but Re(VII) reduction would require a lower E_h. Thus, the use of Re as a Tc analogue is only applicable under aerobic conditions where both species are expected to remain as an oxyanion (+7 oxidation state).

This study highlights the dependence of selectivity on ion size and charge. Additionally, the variation of the sodalite structural parameter as a function of composition (anion mixing) will shed light on the extent of anion incorporation into mixed sodalites formed in environmentally relevant conditions such as subsurface and engineered wastes, vitrification products, and materials formed by chemical weathering.

2. Materials and Methods

2.1. Hydrothermal Mineral Synthesis

Mixed-anion sodalites with ReO_4^- and one other anion (X^{n-}) were hydrothermally synthesized based on modification of a method previously described by Liu and Navrotsky (2007): sodium hydroxide (Alfa Aesar) was mixed with zeolite 4A ($Na_{12}Al_{12}Si_{12}O_{48}{\cdot}xH_2O$, W.R. Grace & Co.) and sodium salts of the appropriate anions. The zeolite supplied a 1:1 molar ratio of Si/Al. The mixed sodalites were synthesized in a 60-mL Teflon digestion bomb filled with 20 mL of deionized water, one gram of NaOH pellets (1.25 *M* NaOH) and 0.5 g of zeolite. To these basic solutions, 0.88 *M* of $NaReO_4$ was added and 0.88 *M* of Cl^-, CO_3^{2-}, SO_4^{2-}, MnO_4^-, or WO_4^{2-} was added as the competing anion. The rationale for the concentrations used in this experiment was that we wanted to produce pure sodalite phases to determine anion selectivity in a mixed system. All chemical reagents were used as received.

To perform hydrothermal syntheses, the bombs were capped, and reagents were aged for 96 h in a 90 °C oven. After decanting the basic supernatant solutions, the solid precipitates were washed three times with deionized water (0.054×10^{-3} dSm^{-1}) by centrifugation. The solids were dialyzed in deionized water until the electrolytic conductivity was ≤0.01 dSm^{-1}, dried for 24 h, and weighed. Solid yield after dialysis ranged from 0.5 to 0.6 g.

2.2. Powder X-ray Diffraction

X-ray diffraction data were obtained with a Panalytical Xpert Pro diffractometer (XRD) scanning at 1.5 °/min over 5 – 90° 2θ. We used CoK_α radiation (λ = 1.789010 Å) and an X'Celerator silicon strip detector equipped with an Fe filter. Scans used ¼° fixed

divergence slits and ½° anti-scatter slits. Jade and/or High Score Plus software, and the ICDD database were used for mineral identification (Kabekkodu, 2012). Rietveld refinements of the XRD data were performed in High Score Plus and/or GSAS with EXPGUI interface (Toby, 2001) using the reported structures of the following phases: $Na_8(AlSiO_4)_6(NO_2)_2$, $Na_8(AlSiO_4)_6(ReO_4)_2$, and $Na_6Ca_{1.5}(AlSiO_4)_6(CO_3)_{1.5}(H_2O)_{1.75}$ (Buhl et al., 1996; Hackbarth et al., 1999; Mattigod et al., 2006). The following parameters were allowed to vary: the background (8 parameters), unit cell, Na position, peak shape (5 parameters: U, V, W, and two peak shape parameters), overall thermal parameter (B), and preferred orientation.

2.3. X-ray Absorption Near Edge Structure (XANES) Spectroscopy

Powdered sodalite samples were mixed with boron nitride and mounted on an aluminum holder with Kapton windows. The XANES spectra were obtained at the Stanford Synchrotron Radiation Lightsource (SSRL) using the 11-2 beamline equipped with a Si (220) double crystal monochromator (Φ = 90 crystals) detuned 50% to reduce the harmonic content of the beam. The spectra from 0.2 keV below to 10 keV above the Re L_2-edge (11.959 keV) were collected either in transmission mode using nitrogen-filled ion chambers or fluorescence mode using a 100-element Ge detector and corrected for detector dead time. We converted raw data to spectra and normalized with SixPack and Artemis (Ravel and Newville, 2005). Normalized XANES spectra were fit using standard spectra in the locally written program 'fites', which utilizes a non-linear least squares approach to fitting data (Li et al., 1995). Two reference spectra, ReO_2(s), and pure ReO_4-sodalite, were used for data fitting. The XANES spectra of the samples were allowed to vary in energy during fitting, and the spectral resolution is 7 eV based

153 on the width of the white line at the Re L_2-edge. Henceforth, we will refer to "ReO_4^-" in
154 the mixed sodalites as "Re" because no other "Re" species are significant in this study.

155 **2.4. Electron Microscopy**

156 Scanning electron micrographs (SEM) were obtained with platinum-palladium
157 sputter-coated powder sodalite samples. The coated samples were examined using a
158 field emission scanning electron microscope (FESEM) with an accelerating voltage of
159 30 keV, and a resolution of 1 nm. The FESEM was equipped with a field emission gun
160 (FEI Quanta 200F, FEI Co., Hillsboro, OR) and Everhart-Thornley detector.

161 **2.5. Chemical Analysis**

162 The powder sodalite samples digested in 3% nitric acid were analyzed for Na
163 concentrations by atomic emission and absorption spectrophotometry (Varian 220
164 Flame Atomic Absorption Spectrometer, Varian Ltd., Mulgrave, Australia). The Si, Al,
165 Mn, W, and Re concentrations in the solids were determined by inductively coupled
166 plasma-mass spectrometry (Agilent 7700 ICP-MS, Santa Clara, CA), and
167 concentrations of Cl^- and, SO_4^{2-} by ion chromatography (HPLC-10Ai, Shimadzu Inc.,
168 Canby, OR). Total carbon concentration was determined by dry combustion from
169 TruSpec C/N analyzer (Leco Corporation, St. Joseph, MI) equipped with a high
170 temperature combustion method and infrared detection technique.

171 **3. Results**

172 **3.1. Synthesis Product Morphology**

173 The SEM images of the mixed-anion sodalites are shown in Fig. 2. The mixed-anion
174 sodalites formed in the presence of Cl^-, CO_3^{2-}, MnO_4^- and WO_4^{2-} were hexagonal
175 crystallites (Fig. 2A-B, D-E). The observed morphology differs from the lepispheric

morphology (i.e., thin disks or blades) reported by Deng et al. (2006) for precipitates formed from simultaneous additions of two or more anions (Cl^-, NO_2^-, NO_3^-, CO_3^{2-}, SO_4^{2-}, PO_4^{3-}) to starting solutions of Na hydroxide, aluminate, and silicate. In contrast, our experiments used zeolite as the source for Al and Si. The crystalline solids formed in the presence of SO_4^{2-} anions were dominated by lepispheric and/or lenticular-shaped crystal structures (Fig. 2C). The observed Re/SO_4-sodalite morphology was similar to those reported by Deng et al, (2006) for precipitates formed in binary or multi-anion solutions.

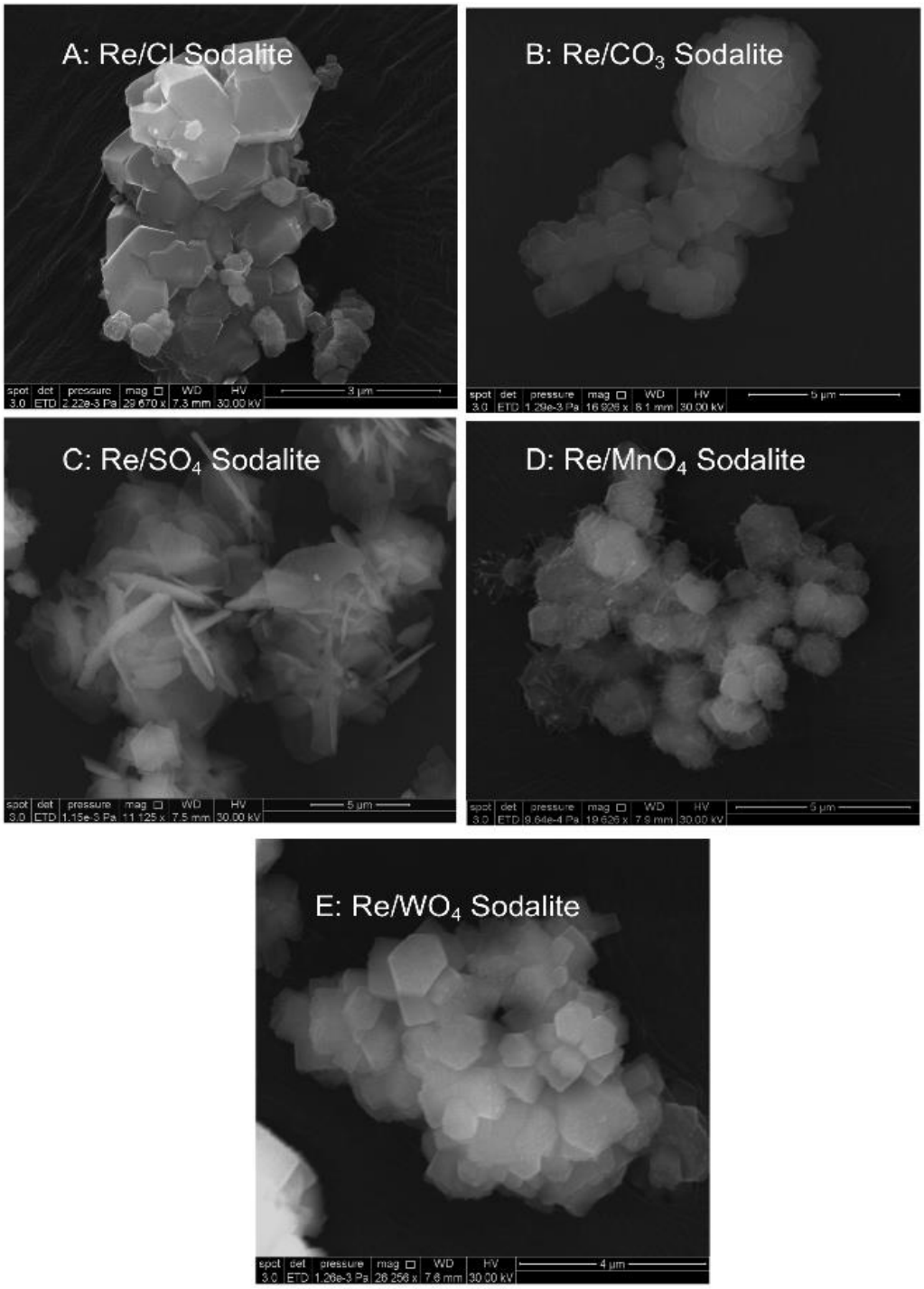

184

185 **Fig. 2.** SEM images of mixed-anion sodalite formed in an equimolar ReO_4^-/ X^{n-} solution. Images

186 scale bars are between 3 – 5μm

187

188

3.2. Composition Analysis

The chemical composition of the synthesized products is shown in Table 1. The mixed-anion sodalites contained from 0.02 – 1.90 moles of ReO_4^- and 0.04 – 2.10 moles of X^{n-} per formula unit. The sodalites, synthesized in the presence of ReO_4^- and Cl^-, CO_3^{2-}, or SO_4^{2-} incorporated negligible amounts of ReO_4^-. In contrast, the sodalite cages exhibited strong preference for ReO_4^- over WO_4^{2-} with ~95% ReO_4^- occupancy of available sites. Further evidence of ReO_4^- incorporation into sodalite is shown in the energy-dispersive X-ray spectroscopy (EDS) patterns (Fig. 3). Perrhenate was best incorporated into the Re/MnO_4- and Re/WO_4-sodalites whereas insignificant incorporation occurred for the Re/Cl-, Re/SO_4- and Re/CO_3-sodalites.

Table 1.

Chemical composition data for mixed-anion sodalites (mol/formula unit).

Structural Formula	Na	Al	Si	Re/X	ReO_4	X*
$Na_8[Al_6Si_6O_{24}](Cl_{(2.1)}ReO_{4(0.003)})$	7.96 ±0.16	6.00 ±0.05	6.06 ±0.11	0.00	0.003 ±0.001	2.14 ±0.07
$Na_8[Al_6Si_6O_{24}](CO_{3(1.0)}ReO_{4(0.02)})$	8.00 ±0.30	6.01 ±0.11	6.00 ±0.10	0.02	0.021 ±0.005	1.01 ±0.10
$Na_{7.6}[Al_6Si_6O_{24}](SO_{4(0.96)}ReO_{4(0.08)})$	7.61 ±0.07	6.02 ±0.07	6.08 ±0.07	0.08	0.080 ±0.002	0.958 ±0.12
$Na_8[Al_6Si_{5.9}O_{24}](MnO_{4(1.1)}\ ReO_{4(0.97)})$	8.09 ±0.17	6.09 ±0.05	5.92 ±0.02	0.89	0.965 ±0.015	1.09 ±0.03
$Na_{7.9}[Al_6Si_6O_{24}](WO_{4(0.05)}ReO_{4(1.9)})$	7.94 ±0.10	6.02 ±0.08	6.00 ±0.17	39.7	1.904 ±0.03	0.048 ±0.004

*X: Anions (Cl^-, CO_3^{2-}, SO_4^{2-}, MnO_4^-, WO_4^{2-}).

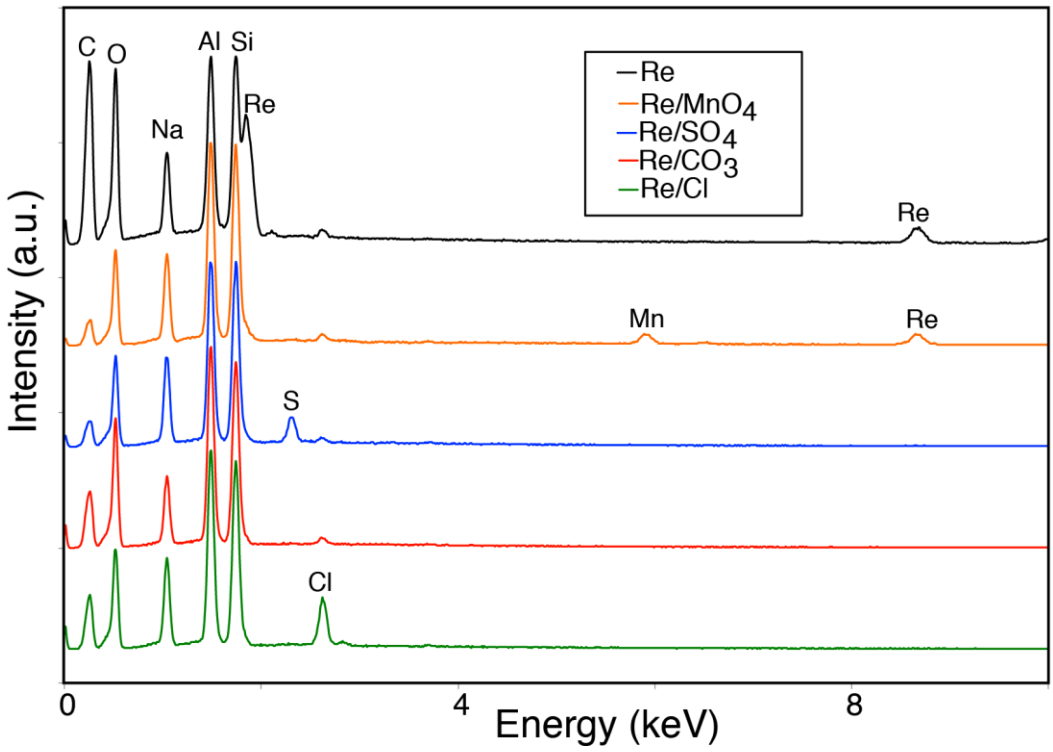

Fig. 3. EDS spectra of select mixed-anion sodalites. The Re/WO_4 spectrum is not shown. The additional Cl^- peaks in some of the samples are from the epoxy matrix used in thin section preparation.

3.3. Mineral Structure

The calculated XRD patterns obtained from the Rietveld refinements of the mixed-anion sodalites are displayed in Fig. 4. The refined lattice parameter (*a*) and index of agreement (χ^2) for the mixed-anion sodalites are shown in Table 2. The lower the χ^2 term the better the fit. The space group $P\bar{4}3n$ was adopted for the mixed-anion sodalites with (*a*) ranging from 8.8885(2) to 9.1527(1) Å. The Rietveld refinements indicate that minor amounts of cancrinite (<2 wt%) were formed along with the dominant sodalite phase(s).

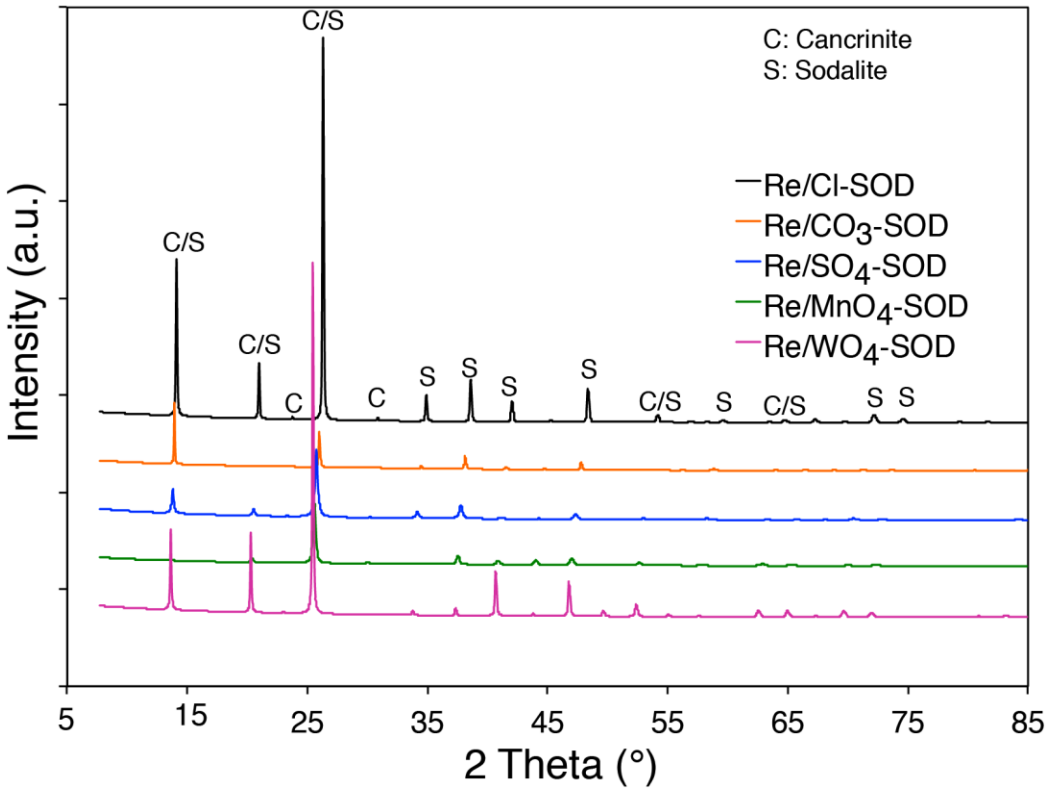

Fig. 4. Refined (calculated) powder X-ray spectra for mixed-anion sodalites.

Table 2.

Refined powder X-ray data for mixed-anion sodalite.

Sample Type	Structural Formula	*a* (Å)	esd	χ^2
Re/Cl-SOD	$Na_8[Al_6Si_6O_{24}](Cl_{(2.1)}ReO_{4(0.003)})$	8.8885	±0.0002	2.76
Re/CO_3-SOD	$Na_8[Al_6Si_6O_{24}](CO_{3(1.0)}ReO_{4(0.02)})$	8.9691	±0.0002	8.07
Re/SO_4-SOD	$Na_{7.6}[Al_6Si_6O_{24}](SO_{4(0.96)}ReO_{4(0.08)})$	9.0785	±0.0004	3.60
Re/MnO_4-SOD	$Na_8[Al_6Si_{5.9}O_{24}](MnO_{4(1.1)} ReO_{4(0.97)})$	9.1258	±0.0005	1.32
Re/WO_4-SOD	$Na_{7.9}[Al_6Si_6O_{24}](WO_{4(0.05)}ReO_{4(1.9)})$	9.1527	±0.0002	6.05

a – unit cell parameter, esd – estimated standard deviation, and χ^2 – index of agreement.

3.4. Rhenium Oxidation State

The spectra fitting were performed as described by Lukens et al. (2005). The Re L_2-edge XANES data were fitted using only the spectra of ReO_2(s) and ReO_4-sodalite (Pierce et al., 2014, submitted). The spectrum of Re/MnO_4-sodalite is presented in Fig. 5. In the mixed-anion sodalites, the spectrum of ReO_4-sodalite contributes significantly (≥92%) to the fit and only in the presence of Cl^- does the spectrum of ReO_2(s) contribute significantly to greater than 2σ of the fit (Table 3). Thus, the ReO_4^- species is considered the dominant rhenium species in these solid phases.

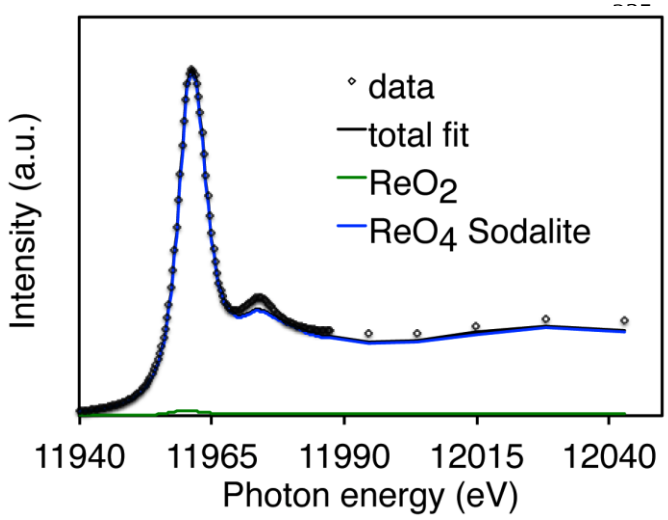

Fig. 5. Rhenium L_2-XANES spectral data for Re/MnO_4-sodalite; data are represented by dots, and the fit is shown by the black line. Results indicate that the Re(VII) oxidation state dominates.

Table 3.

Rhenium L_2-edge XANES spectral fitting results for mixed-anion sodalites.

Sample	ReO_2‡	*p**	ReO_4-sodalite‡	*p**
Re/Cl-SOD	0.18(6)†	0.017	0.82(5)	<0.001
Re/CO_3-SOD	0.08(5)	0.168	0.92(4)	<0.001
Re/SO_4-SOD	0.03(5)	0.545	0.97(4)	<0.001
Re/MnO_4-SOD	0.02(6)	0.828	0.98(5)	<0.001
Re/WO_4-SOD	0.00(2)	1.000	1.00(1)	<0.001

‡The fractional contributions of each oxidation state to the XANES spectral.

†The number in parentheses is the standard deviation in the same decimal place as the digit preceding it.

*p is the usual p-value, which is the likelihood that the improvement to the fit due to inclusion of this component is due to random error (noise) in the data. If $p < 0.05$, then the data supports the hypothesis that a given component is present (improvement is > 2δ□of the fit).

4. Discussion

4.1. Incorporation of ReO_4^- in the Presence of Competing Anion (X^{n-})

Using an equimolar concentration of ReO_4^- and X^{n-} in the starting solutions, we synthesized five mixed-anion sodalites and tested the hypothesis that ion size and charge drive the selectivity for a given anion.

As the ionic radius increases in the following series: $Cl^- < CO_3^{2-} < SO_4^{2-} < MnO_4^- < WO_4^{2-}$, the selectivity of ReO_4^- for the mixed sodalite linearly increased, consistent with the linear expansion of the cages from the Re/Cl-sodalite to the Re/WO_4-sodalite.

The inability to form mixed sodalites containing significant amounts of ReO_4^- in the presence of Cl^-, CO_3^{2-}, and SO_4^{2-} is due the large size difference between ReO_4^- and the competing anions, and the nature of the anions. According to Hume-Rothery Rules, the following conditions favor the formation of solid solutions (e.g., metal alloys, crystallized salts): similarity in ion crystal structures, valency, electronegativity and size (Mizutani, 2010). Sodalite cages can host anions of varying size due to cooperative tilting and deformation of the frameworks up to a point. Trill et al. (2003) state that the difference in anion size may not exceed 15%, because of excessive strain imposed on the sodalite framework when anions of different size are accommodated. This behavior is confirmed in our system as shown in Fig. 6, where anion selectivity is plotted against the difference in ionic radii (DIR) of solvent A (r_A) and solute B (r_B) where:

$$\mathrm{DIR}\ (\%) = \left(\frac{r_A - r_B}{r_B}\right) \times 100$$

As the DIR increases from 2.7% in the Re/WO_4-sodalite to 51.2% in the Re/Cl-sodalite, the ReO_4^- distribution coefficient exponentially declines from 3.73 to 0.02. When the DIR between ReO_4^- and the competing anion exceeds 15%, the concomitant inclusion of both anions would sufficiently distort the mixed-anion sodalite cages, resulting in the exclusion of the larger anion from the cages. This trend is manifested in the preferential formation of mostly Cl-, CO_3- and SO_4-sodalites containing minor amounts of enclathrated ReO_4^-. Although the DIR for Re/SO_4 (13%) and Re/WO_4-sodalites (2.7%) should favor the formation of mixed sodalite solid solutions, the distribution coefficient shows a clear preference for SO_4^{2-} and ReO_4^- respectively. In the case of SO_4^{2-}, the DIR is close to 15%, indicating that this difference is still large

enough to strongly favor the smaller anion. For WO_4^{2-}, the difference in charge and inability to fill all cages with either ReO_4^- or WO_4^{2-} may explain the preference for ReO_4^-.

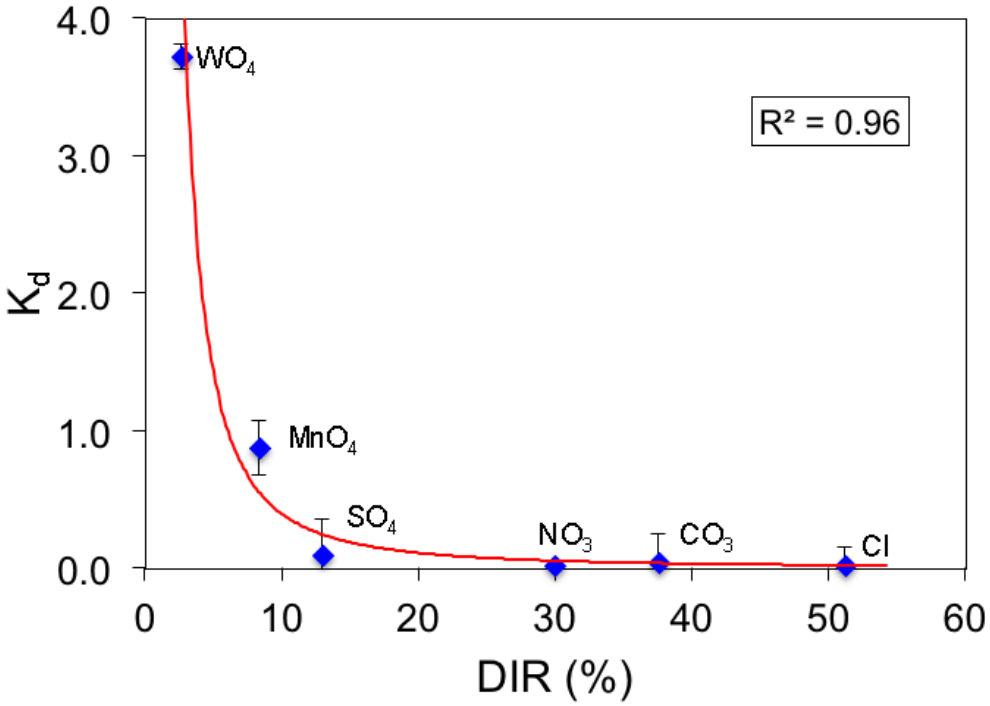

Fig. 6. The distribution coefficient (K_d) graph for ReO_4^- sequestered in mixed-anion sodalites as a function of the DIR. Generally, more than 90% of sodalite cages are filled with anions. *NO_3 data point is from Dickson et al. (2014)

Table 4.

Ionic radii, hydration energy and ionic potential data for studied anions with respect to ReO_4^-.

Anions (X)	r (nm)	DIR (%)	Ionic Potential (Z/r)	Hydration Energies ($kJmol^{-1}$)
Cl^-	0.172[d]	51.2	0.58	-340[a]
CO_3^{2-}	0.189[c]	37.6	1.06	-1315[a]
SO_4^{2-}	0.230[a]	13.0	0.87	-1080[a]
NO_3^-	0.200[a]	30.0	0.50	-300[a]
MnO_4^-	0.240[a]	8.3	0.42	-235[a]
WO_4^{2-}	0.267[b]	2.7	0.75	-702[e]
ReO_4^-	0.260[a]	0.0	0.39	-330[a]
TcO_4^-	0.252[d]	3.2	0.40	-251[d]

r represents the ionic radii of anions

[a] Thermodynamics of solvation of ions; Marcus et al. (1991)

[b] Ionic radius in aqueous solution; Marcus et al. (1988)

[c] Handbook of chemistry and physic; David et al. (2003)

[d] Physical factors in anion separation; Moyer et al. (1979)

[e] Hydration and extraction of oxyanion; Abramov et al. (2001)

DIR: Difference in ionic radii.

5. Conclusions and Implications for ^{99}Tc Immobilization

In this study, five mixed-anion sodalites containing extra-framework species were synthesized and characterized. The selectivity for intra-lattice anions of the products was highly dependent on the size and, to a lesser extent, the charge of the competing anion. The results of our study suggest that similarity in ionic radius (DIR of ≤15%) and charge (ionic potential) promote the competitive incorporation of ReO_4^- into the mixed-

anion sodalites (Fig. 6 and Table 4). Selectivity of ReO_4^- for the mixed-anion sodalites was found to increase in the series as follows: $Cl^-<CO_3^{2-}<NO_3^-<SO_4^{2-}<MnO_4^-<WO_4^{2-}$.

The findings in this study have implications for the fate and transport of $^{99}TcO_4^-$ in subsurface sediments, assuming that its chemical behavior can be well approximated by ReO_4^-. Firstly, the formation of a Re/MnO_4-sodalite solid solution implies that ReO_4^- is a suitable analogue for TcO_4^-. Like TcO_4^-, MnO_4^- shares a similar size, and ionic potential with ReO_4^- (Table 4). The distribution coefficient for ReO_4^- was unity, implying nearly equal selectivity for MnO_4^- and ReO_4^- during the formation of sodalite. The same is likely true for TcO_4-sodalite.

Secondly, our results also suggest that while neoformed feldspathoid minerals, such as sodalite, can incorporate ^{99}Tc as TcO_4^-, but smaller competing anions with DIR >12% will be preferred. Unfortunately, in many instances where environmental conditions are conducive for feldspathoid formation, the waste solutions may also contain high concentrations of such competing anions.

One limitation of our results is that sodalite synthesis occurred in a closed system. In open, free-flowing systems, the smaller anions may become depleted leaving TcO_4^- to be incorporated later in the reaction sequence. Additionally, our experiments were designed specifically to form only sodalite phases because of the ability of its cages to sequester large ions such as TcO_4^-. In other systems, neoformed mineral phases could include cancrinite, zeolite, nosean, and nepheline. It has been reported that NO_3^- is sequestered by cancrinite and SO_4^{2-} by nosean, whereas Cl^- and ReO_4^- are incorporated into mixed-anion sodalites (Pierce et al., 2014). Thus, at the comparatively low concentrations of TcO_4^- (10^{-6} to 10^{-4} *M*) expected in most nuclear waste streams,

TcO_4^- could intercalate into the mixed-anion sodalite phases after other competing anions have been selectively sequestered into their respective neoformed mineral phases.

Additionally, to enhance ReO_4^- (and ultimately TcO_4^-) sequestration into mixed sodalites pre-treatment of the waste streams has been suggested to remove NO_3^- and NO_2^- from the wastes prior to formation of sequestering aluminosilicate phases (Pierce et al., 2014). Although mixed-anion sodalites are somewhat less durable compared to their pure phase analogues (Pierce et al., 2014), they remain an excellent waste form for the long-term disposal of key anion radionuclides in an environment where they are stable—e.g., under the alkaline conditions expected for vitrified waste disposal. For example, Pierce et al. (2014) estimated the leach rate of ReO_4^- from Re-sodalite to be 0.0006 g $m^{-2}d^{-1}$.

Further work is needed in open systems, with a greater range of hydrothermal conditions (high temperature and dynamic flow synthesis of an array of aluminosilicate mineral phases), and at realistic ^{99}Tc concentrations, to mimic waste-impacted subsurface sediments and managed waste streams to determine if mixed-anion sodalites may be relevant sequestering phase(s).

Acknowledgements

This material is based upon work supported by the U.S. Department of Energy (DOE), Office of Science, Biological and Environmental Research Program (SBER), and was performed at Washington State University under contract No. DE-PS02-09ER65075 and at Oak Ridge National Laboratory under contract No. DE-AC05-00OR22725. Portions of this work were supported by DOE, Office of Science, Basic

Energy Sciences, Chemical Sciences, Biosciences, and Geosciences Division, Heavy Element Chemistry Program and were performed at Lawrence Berkeley National Laboratory under contract No. DE-AC02-05CH11231. Portions of this work were performed at the Stanford Synchrotron Radiation Lightsource (SSRL), which is a DOE office of Science user facility operated by Stanford University. We are also indebted to the staff at the Franceschi Microscopy and Imaging Center at Washington State University for access to and assistance with the use of their SEM facilities. We also acknowledge financial support from the Mineralogical Society of America and the Bullitt Foundation.

References

Baerlocher, C. and McCusker, L. B.: Database of zeolite structures. http://www.iza-structure.org/databases, 2014.

Brenchley, M. E. and Weller, M. T.: Synthesis and structures of $M_8[AlSiO_4]_6(XO_4)_2$, M=Na, Li, K, X=Cl, Mn Sodalites, Zeolites, 14, 682-686, 1994.

Buhl, J. C., Reich, D., Mundus, C., and MullerWarmuth, W.: Si-29 MAS NMR investigations on the crystallization of nitrite-sodalite, React. Kinet. Catal. Lett., 58, 13-18, 1996.

Custelcean, R. and Moyer, B. A.: Anion separation with metal-organic frameworks, Eur. J. Inorg. Chem., doi: 10.1002/ejic.200700018, 2007. 1321-1340, 2007.

Darab, J. G. and Smith, P. A.: Chemistry of technetium and rhenium species during low-level radioactive waste vitrification, Chem. Mater., 8, 1004-1021, 1996.

Deng, Y. J., Harsh, J. B., Flury, M., Young, J. S., and Boyle, J. S.: Mineral formation during simulated leaks of Hanford waste tanks, Appl. Geochem., 21, 1392-1409, 2006.

Dickson, J. O., Harsh, J. B., Flury, M., Lukens, W. W., and Pierce, E. M.: Competitive incorporation of perrhenate and nitrate into sodalite, Environ. Sci. Technol., 48, 12851-12857, 2014.

Ewing, R. C.: The nuclear fuel cycle: A role for mineralogy and geochemistry, Elements, 2, 331-334, 2006.

Ewing, R. C.: Nuclear waste forms for actinides, Proceedings of the National Academy of Sciences of the United States of America, 96, 3432-3439, 1999.

Hackbarth, K., Gesing, T. M., Fechtelkord, M., Stief, F., and Buhl, J. C.: Synthesis and crystal structure of carbonate cancrinite $Na_8(AlSiO_4)_6CO_3 3.4H_2O$, grown under low-temperature hydrothermal conditions, Microporous Mesoporous Mater., 30, 347-358, 1999.

Icenhower, J. P., Qafoku, N. P., Zachara, J. M., and Martin, W. J.: The biogeochemistry of Technetium: A review of the behavior of an artificial element in the natural environment, American Journal of Science, 310, 721-752, 2010.

Johnson, G. M., Mead, P. J., and Weller, M. T.: Structural trends in the sodalite family, PCCP, 1, 3709-3714, 1999.

Kabekkodu, S. N. (Ed.): PDF-4/Minerals database, International Center for Diffraction Data, Newtown Square, PA, USA, 2012.

Li, G. G., Bridges, F., and Booth, C. H.: X-ray-absorption fine-structure standards: A comparison of experiment and theory Physical Review B, 52, 6332-6348, 1995.

Liu, Q. and Navrotsky, A.: Synthesis of nitrate sodalite: An in situ scanning calorimetric study, Geochim. Cosmochim. Acta, 71, 2072-2078, 2007.

Lukens, W. W., Bucher, J. J., Shuh, D. K., and Edelstein, N. M.: Evolution of technetium speciation in reducing grout, Environmental Science & Technology, 39, 8064-8070, 2005.

Lukens, W. W., McKeown, D. A., Buechele, A. C., Muller, I. S., Shuh, D. K., and Pegg, I. L.: Dissimilar behavior of technetium and rhenium in borosilicate waste glass as determined by X-ray absorption spectroscopy, Chem. Mater., 19, 559-566, 2007.

Maddrell, E., Gandy, A., and Stennett, M.: The durability of iodide sodalite, J. Nucl. Mater., 449, 168-172, 2014.

Marcus, Y.: Thermodynamics of solvation of ions. Part 5 - Gibbs free energy of hydration at 298.15-K Journal of the Chemical Society-Faraday Transactions, 87, 2995-2999, 1991.

Mattigod, S. V., McGrail, B. P., McCread, D. E., Wang, L. Q., Parker, K. E., and Young, J. S.: Synthesis and structure of perrhenate sodalite, Microporous Mesoporous Mater., 91, 139-144, 2006.

Mizutani, U.: Hume-Rothery Rules for Structurally Complex Alloy Phases, Taylor & Francis, Boca Raton, FL, 2010.

Moyer, B. A. and Bonnesen, P. V. (Eds.): Physical Factors in Anion Separation. Supramolecular chemistry of anions, Wiley-VCH, New York, 1979.

Pierce, E. M., Lilova, K., Lukens, W. W., Navrotsky, A., Fritts, J., Rawn, C., Jantzen, C. M., Missimer, D. M., and Huq, A.: Structure and thermochemistry of perrhenate sodalite and perrhenate/pertechnetate guest-guest sodalite, Proceeding of the national Academy of Science, 2014, submitted.

Pierce, E. M., Lukens, W. W., Fitts, J. P., Jantzen, C. M., and Tang, G.: Experimental determination of the speciation, partitioning, and release of perrhenate as a chemical

surrogate for pertechnetate from a sodalite-bearing multiphase ceramic waste form, Appl. Geochem., 42, 47-59, 2014.

Ravel, B. and Newville, M.: Athena, Artemis, Hephaestus: Data analysis for X-ray absorption spectroscopy using Ifeffit, Journal of Synchrotron Radiation, 12, 537-541, 2005.

Stein, A., Ozin, G. A., and Stucky, G. D.: Class-B sodalites - Nonstoichiometric silver, sodium halosodalites, JACS, 114, 8119-8129, 1992.

Taylor, D. and Henderson, C. M. B.: A computer model for the cubic sodalite structure, Phys. Chem. Miner., 2, 325-336, 1978.

Toby, B. H.: EXPGUI, a graphical user interface for GSAS, J. Appl. Crystallogr., 34, 210-213, 2001.

Trill, H.: Sodalite solid solution systems: Synthesis, topotactic transformations, and Investigation of framework-guest and guest-guest interactions, PhD Dissertation, Universität Münster, 187 pp., 2002.

Wakoff, B. and Nagy, K. L.: Perrhenate uptake by iron and aluminum oxyhydroxides: An analogue for pertechnetate incorporation in Hanford waste tank sludges, Environmental Science & Technology, 38, 1765-1771, 2004.

Weller, M. T. and Wong, G.: Mixed halide sodalites, Eur. J. Solid State Inorg. Chem., 26, 619-633, 1989.

Weller, M. T., Wong, G., Adamson, C. L., Dodd, S. M., and Roe, J. J. B.: Intracage reactions in sodalites, Journal of the Chemical Society-Dalton Transactions, doi: 10.1039/dt9900000593, 1990. 593-597, 1990.